A composite seismic source model for the first major event during the 2022 Hunga (Tonga) volcanic eruption

Jinyin Hu[1, *], Thanh-Son Phạm[1] and Hrvoje Tkalčić[1]

[1]Research School of Earth Sciences, The Australian National University, Canberra, ACT, Australia

[*]Corresponding author: Jinyin Hu (jinyin.hu@anu.edu.au)

Key Points:

- We perform probabilistic inversion of seismic waveform data to study the force equivalent system of the 2022 Hunga (Tonga) eruption.
- The first major explosive event of the shallow eruption sequences consists of an explosive moment tensor and a large upward force.
- A possible mechanism of the accopanying upward force is the rebound force responding to the sudden pressure drop of uplifted water body.

Abstract

The violent eruption of the Hunga (Tonga) submarine volcano on 15 January 2022 caused a 58 km-heigh ash plume, catastrophic tsunami, and significant global seismic and infrasound waves. However, the physical mechanism underpinning its multiple-explosive events remains unclear, and its resolvability relies on the seismic waveform source inversion. The studies of two different point-source models, the seismic moment tensor (MT) and the single force (SF), have been performed separately for this eruption, which, interestingly, can explain the seismic data adequately. Here, we use a joint inversion of MT and SF to unravel a composite source of an explosive MT and a significant upward force for the first major explosive event. Regarding the direction and magnitude, we propose that the upward force is likely a rebound force in response to the pressure drop on the seafloor because the water body above the volcano was abruptly uplifted by the shallow underwater explosion.

Plain Language Summary

The physical process of the violent eruption of the Hunga (Tonga) submarine volcano on 15 January 2022 remains unclear. To date, the common source model for volcano eruptions – a single force (SF) and the common source model for earthquakes and explosions – a moment tensor (MT), have been inferred individually for this eruption. Interestingly, both can explain the recorded seismic signals reasonably well. A question arises whether a combination of sources is a better physical model. Therefore, we combine the MT and SF to represent the eruption process in this study. The source analysis for the first major event of this eruption reveals a composite process of a shallow underwater explosion and a significant upward force. The upward force is opposite the common downward-reaction force to the material jetting. It is likely caused by the abrupt displacement of the water above the volcano resulting from the shallow underwater explosion. When the downward water pressure on the seafloor vanishes, the seafloor responds by an upward-rebound force.

1 Introduction

On 15 January 2022, the catastrophic eruption of Hunga, a submarine volcano in the Tongan archipelago in the southern Pacific Ocean, occurred. The violent phase started at 04:14:45 UTC, as reported by the U.S. Geological Survey (USGS, 2022). The volcanic plume reached into the mesosphere to ~58 km high (Matoza et al., 2022; Proud et al., 2022). The events triggered sea waves, including ashfall and tsunamis as high as 45 m near the Tonga kingdom (Carvajal et al., 2022; Kubota et al., 2022; Lynett et al., 2022; Omira et al., 2022; Purkis et al., 2023). This eruption also generated significant seismic waves recorded on seismic stations globally (e.g., Donner et al., 2023; Tarumi & Yoshizawa, 2023). The rapid estimate of the volcanic explosivity index is about 5 ~ 6 (Poli & Shapiro, 2022; Yuen et al., 2022), making it one of the largest eruptions ever recorded instrumentally.

Ongoing progress has been made in understanding the dynamic model, or the equivalent seismic force system, of the main eruptive events (e.g., 04:15 UTC and subsequent events within 5 minutes), which could shed light on the explosive mechanisms of the eruptions. However, the main obstacle to an ultimate understanding of the dynamical model is the lack of in situ seismic observations of the submarine events, where the nearest seismic signals are recorded several hundred kilometers away. Two possible candidate models, including equivalent single force and the seismic moment tensor models, differ intrinsically. The moment tensor does not exert effective net torque to the solid Earth, while the single force does (Julian et al., 1998). A simplified model with a single force dominating an implosive moment tensor was proposed for the St. Hellen volcanic eruption (Kanamori et al., 1984; Kanamori & Given, 1982). Consequently, this model was quickly employed for the Hunga eruption in early seismic studies (Donner et al., 2023; Garza-Girón et al., 2023; Poli & Shapiro, 2022; Yuen et al., 2022; Zheng et al., 2023).

However, more recently, Thurin & Tape (2023) demonstrated that the fit of far-field seismic waveforms can be well satisfied by either upward or downward single force or explosive (i.e., seismic source involving sudden volumetric expansion) or implosive (i.e., seismic source involving sudden volumetric contraction) moment tensor mechanisms. The arguable ambiguity motivated an independent line of work considering seismic moment tensors with dominating isotropic components as the physical model of the explosion (Thurin & Tape, 2023; Thurin et al., 2022). Given the ambiguity, a possible joint moment tensor and single force model could provide a more feasible explanation for the eruptive events but has not been formally considered in literature yet, possibly due to high computational costs. However, such a joint model has been suggested to hold the key to a feasible dynamical model of the climactic submarine eruption (Thurin & Tape, 2023; Yuen et al., 2022).

In this study, we build upon our method development (Hu et al., 2023) to address the problem, jointly inverting the MT and SF components for the Hunga eruption (Figure 1). The inversion method is hierarchical because the station-specific noise amplitudes and time-shifts were inverted as hyperparameters alongside the source parameters. The time-shift parameters were used to account for waveform mismatch between simulated and observed seismic waveforms. This method was demonstrated to be effective in resolving the non-double-couple components of shallow seismic sources, as in the case of DPRK explosions (Hu et al., 2023). As a result, we show that the composite model made of an isotropic-dominant MT and a vertical upward force, interpreted as an instant rebound force due to the upward displacement of the water body, is a preferred explanation of the source process.

2 Results of the Joint Source Inversion

We focus on the first main event, E1 in Figure 1(b) which tries to reproduce the stacked ground vertical displacement from Yuen et al. (2022) by using phase-weighted stack (Schimmel & Paulssen, 1997) with a smaller dataset. E1 is the most significant event on January 15, and separate it from other subevents as we use the point source approximation

2.1 Joint moment tensor and single force hierarchical Bayesian inversion

To gain more insights into the Hunga eruption source process, we developed a Bayesian joint inversion of MT and SF using regional surface waves in this study. First, a broader range of source processes considering a composite source representation of SF and MT is explored, as has been conducted for other volcanic eruptions (e.g., Chouet et al., 2003; Dreger et al., 2000; Duputel & Rivera, 2019; Lanza & Waite, 2018; Ohminato et al., 1998; Tkalčić et al., 2009; Uhira & Takeo, 1994). Second, the seismic source inversion includes uncertainty estimate for both data noise and structural error due to the imperfect knowledge of Earth's structures (e.g., Dettmer et al., 2007; Mustać et al., 2020; Phạm & Tkalčić, 2021; Vasyura-Bathke et al., 2021). We use a 1D Earth's model, ak135f (Montagner & Kennett, 1996), but apply time-shifts to re-align observed and predicted waveforms to approximately capture the structural error (Zhao & Helmberger, 1994; Zhu & Helmberger, 1996). Here, time-shifts are treated as station-specific free parameters in the inversion to fully consider their uncertainty (e.g., Hu et al., 2023; Vasyura-Bathke et al., 2020).

The inversion method is built on the Bayesian seismic MT inversion developed by Hu et al. (2023), by extending it for the joint source of MT and SF. In our formulation, the posterior probability is calculated for the following parameters: a composite seismic point-source MT and SF $\mathbf{m}$, station-specific noise $\mathbf{h}$ and time-shifts $\boldsymbol{\tau}$, given the observations $\mathbf{d}_{obs}$. The posterior is proportional to the likelihood function as in Mustać & Tkalčić (2016), Phạm & Tkalčić (2021), and Sambridge et al (2006),

$$p(\mathbf{m}, \mathbf{h}, \boldsymbol{\tau} | \mathbf{d}_{obs}) \propto \frac{1}{\sqrt{(2\pi)^N |\mathbf{C}_{\boldsymbol{e}}|}} exp\left(-\frac{1}{2}(\mathbf{d}(\mathbf{m}, \boldsymbol{\tau}) - \mathbf{d}_{obs})^T \mathbf{C}_e^{-1} (\mathbf{d}(\mathbf{m}, \boldsymbol{\tau}) - \mathbf{d}_{obs})\right) \tag{1}$$

where $\mathbf{m} = \left[M_{xx}, M_{yy}, M_{zz}, M_{xy}, M_{xz}, M_{yz}, F_x, F_y, F_z\right]^T$ for a joint point-source representation of MT and SF, N is the total number of data points; $\mathbf{C}_{\boldsymbol{e}}$ is the block data covariance matrix in which each block corresponds to one seismogram. This posterior probability is sampled by an affine-invariant ensemble samplers (Goodman & Weare, 2010), which effectively and thoroughly explores the joint parameter spaces and possible inter-parameter tradeoffs.

For simplicity, the data noise is assumed uncorrelated, given the relatively good signal to noise ratio of the first subevent E1 (Figure 1b) due to its large magnitude as reported by Donner et al. (2023), and Thurin and Tape (2023). Thus, it can be treated by a block diagonal covariance matrix $\mathbf{C}_{\boldsymbol{e}}$ defined by a set of station-specific noise parameters $\mathbf{h} \coloneqq \{h_i\}$ as,

$$\boldsymbol{C}_i = (h_i \sigma_i)^2 \boldsymbol{I}, \tag{2}$$

where σ_i is pre-computed noise strength from 1-hour pre-event ambient noise. h_i is determined by the data during the inversion.

The shifting of waveforms by $\boldsymbol{\tau}$ is implemented in the frequency domain. For the Hunga eruption, the closest station is about 600 km away, so the travel time difference between Rayleigh and Love waves caused by the polarization anisotropy could be significant. Therefore, we used two unknown time-shifts for each station, one for vertical and radial components and another for tangential component. Thus, the unknown parameter space has in total $(9 + 3 \times n_s)$ dimensions, where the number 3 stems from one noise and two time-shift parameters and n_s is the number of seismic stations. The configuration of inversion e.g., the priors, can be found in Supporting Information S1.

2.2 Recovery tests of composite sources with synthetic data

We tested the method's feasibility to recover three different input shallow sources set arbitrarily at 0.8 km depth: an SF source, an MT source, and their composition, using the real source-station geometry shown in Figure 1(a). For each of the input sources, we conducted three independent inversions using the synthetic data: an MT-only inversion, an SF-only inversion, and a joint inversion. Supporting Information S1 discusses the numerical experiments (Table S1, Figures S1-S9). Here, we summarize the main lessons learned from the experiments to support the interpretation of the real data inversion results in the next section.

Firstly, we observe an ambiguity between the vertical force and isotropic MT as a reasonably good waveform fit can be obtained if one mechanism was assumed in the inversion while the other was indeed used in generating the synthetic data (Figures S2 and S4). This could lead to misinterpreting the source type if MT- or SF-only source type is assumed for the solution (e.g., Donner et al., 2023; Thurin & Tape, 2023).

Secondly, for a joint source mechanism input, both SF- and MT-only inversions resulted in reasonable solutions that comparably explain the data, indicated by the posterior distribution and waveform fit in Figures S7 and S8, respectively. This testifies that a composite source could be misinterpreted if the prior assumption of its nature is not all-inclusive.

Thirdly, the joint MT and SF inversion could reliably resolve the possible composition of different source types, as shown in Figure 2, S3, S6, and S9. For an input composite source of MT and SF (Figure 2), the individual components can be recovered in the joint inversion. The slight linear dependency between vertical force and three MT parameters, M_{xx}, M_{yy}, and M_{zz}, three sub-panels in the lower left corner of Figure 2(a), is caused by the tradeoff between the vertical force and isotropic MT mentioned above. The joint MT and SF inversions also recovered the noise amplitude and the station-specific time-shifts whose true values for all stations are 3 and 0, respectively (Figure 2d).

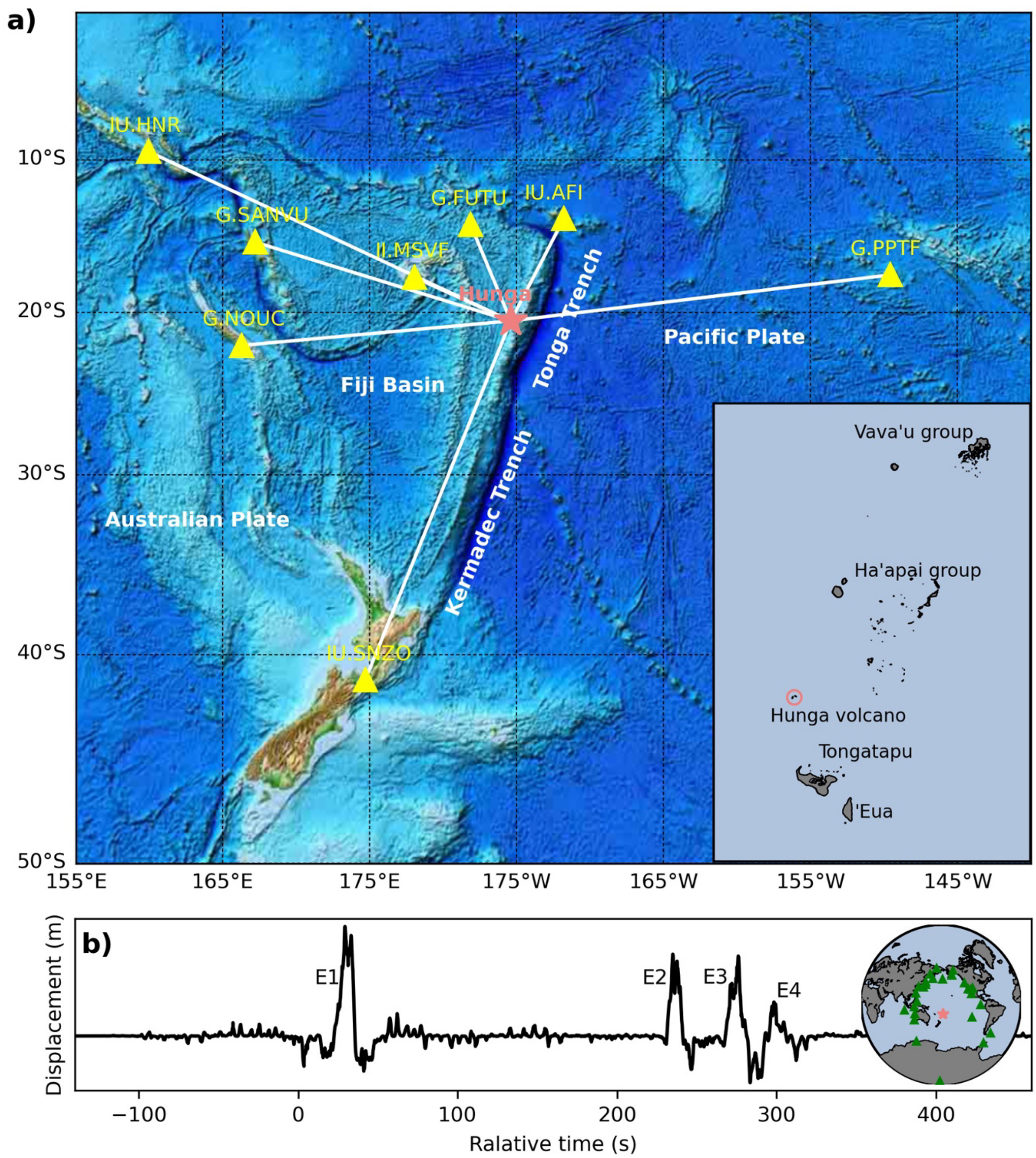

Figure 1: (a) Map of the Tonga-Kermadec arc-trench system, the Hunga volcano (light coral star), and eight broadband stations (yellow triangles) used in this study. A map of the Kingdom of Tonga is plotted at the bottom right corner. (b) The sequence of four subevents showing by the stacked ground vertical displacement at 27 teleseismic stations in Global Seismograph Network (green triangles in the map on right-hand side). Time zero corresponds to the origin time of E1, i.e., 04:14:45 15 January (USGS, 2022).

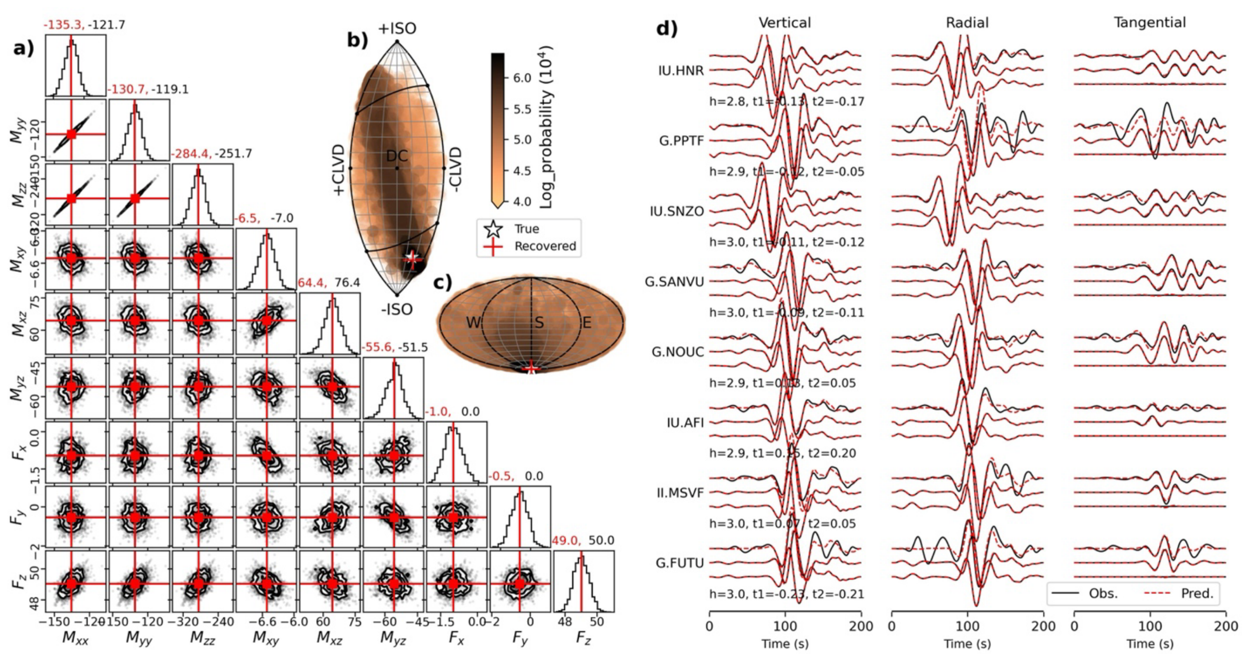

Figure 2: Results of joint MT and SF inversion for the synthetic scenario of a composite source (an implosive MT and downward SF) input. (a) Posterior distribution of the nine source parameters in the convergence stage (defined in Supporting Information S1). The MT and SF parameters units are 10^{16} Nm and 10^{12} N, respectively. Red lines show the mean of each parameter corresponding to the number in red above each column, separated from its true value in black. (b) The lune source-type diagram (Tape & Tape, 2012) with all MTs in the entire inversion stage. (c) The orientations of all forces (Thurin et al., 2022) in the entire inversion stage. The longitude and latitude correspond to force's azimuth and dip angle, respectively. (d) Waveform fit between input (black) and recovered ones (red). The three pairs of waveforms for each component show input and recovered waveforms corresponding to the composite source, its

MT, and SF components. The numbers below each sub-panel are recovered station-specific noise parameters and time-shifts, whose true values are $h = 3$ and $t = 0$, respectively.

2.3 The shallow depth of the Hunga eruption

Insights into the explosion source depth could be important to understand the exact mechanism of the eruptive explosion (Hejrani & Tkalčić, 2020; Kawakatsu, 1996). Constraining the source depth for shallow events is challenging (e.g., Mustać et al., 2018; Mustać & Tkalčić, 2017). Thurin and Tape (2023) performed a grid search for the depth of point-source force and moment tensor individually and found different depth resolutions for different seismic data and source models. They chose 1 km as the preferable source depth by assuming the event happened at the shallow portion of the volcano. According to the bathymetry survey of the National Institute for Water and Atmospheric Research (New Zealand), the seafloor over the volcano caldera pre- and post-eruption indicate that this eruption sequences formed a 0.85 km deep cavern, but the cone rims remain almost untouched (Mackay et al., 2022). This observation motivated us to fix a source depth of 0.8 km in this study.

2.4 Composite source model for the first eruptive event E1

Here, we apply the joint MT and SF inversion for real data of the first major event, E1, in the 2022 eruptive sequence. Details on data preparation and processing can be found in Supporting Information S2. Figure 3 features the inversion results of a composite source with explosive MT and upward SF components. The mean MT suggests a high percentage of the isotropic (ISO) component (62.4%) and a small percentage of the double-couple (DC) component (6.9%), confirming the event's explosive nature. The SF part has a dip angle of -78° (Figure 3c), meaning dominated by an upward force, i.e., $F_z = 2.0 \times 10^{13}$ N.

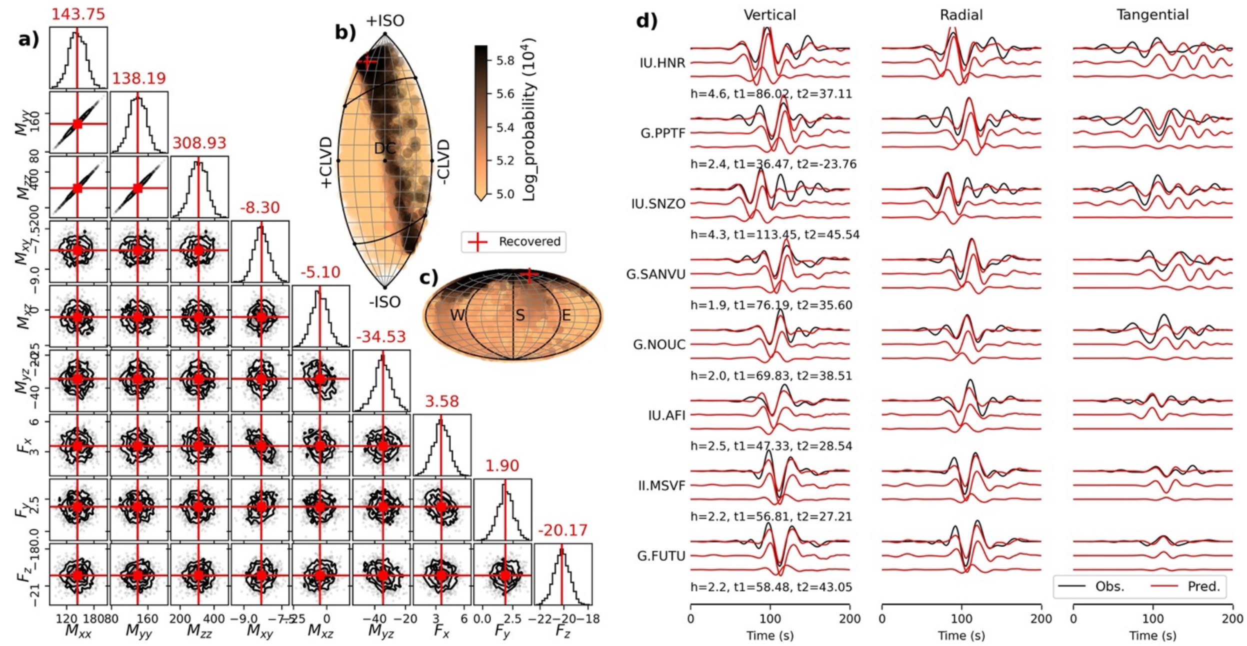

Figure 3. Results of joint MT and SF inversion for the 2022 Hunga first main event E1. (a) The posterior distribution of nine source parameters. Red lines show the mean of each parameter. (b) Evolution of the MT component in the entire inversion stage. (c) Evolution of the SF component in the entire inversion stage. (d) Fit between the observed (black) and predicted waveforms (red). The three predicted waveforms for each component are for the mean composite source of MT and SF, MT component only, and SF component only from the top to the bottom. See the caption of Figure 2 for more details.

This composite source solution of MT and SF is robust based on two other different inversions (rows 4 and 5 in Table S2). In the join MT and vertical force F_z inversion, as shown in Figure S13, a similar explosive MT solution with a high percentage of ISO component (62.5%) and an upward force ($F_z = 1.8 \times 10^{13}$ N) are obtained. The moment magnitude remains $M_w =$ 6.26. The predictions from this composite source can also fit the observation, with a VR only 1% lower than the above source from joint MT and SF inversion. The joint ISO and SF inversion also support the source model of an explosion and an upward force (Figure S14). From the posterior distribution in Figure S14(a), all acceptable SF are upward-directed, and all ISO are positive, pointing to an explosion. This recovered composite source results in a better waveform fit than the SF-only inversion from the comparison in Table S2.

The upward single force is a significant part of the composite source of MT and SF. Here, the contribution of the SF part to the observed waveforms, which is quantified by the ratio of peak-to-peak amplitudes from the SF source and observation, is up to 27%. It also contributes 29% and 35.7% to the observations in the cases of joint MT and F_z inversion and joint ISO and SF inversion, respectively.

The recovered SF component in this work is striking because it is opposite to the downward force obtained by other works (e.g., Garza-Girón et al., 2023; Poli & Shapiro, 2022; Thurin & Tape, 2023) and the SF-only inversion in Figure S12. However, its direction is consistent with the result of Donner et al. (2023). The obtained composite source produces waveforms that match the observations best of all inversions, as shown in Table S2 and plotted in Figure 3(d). We prefer the explanation that the single force component represents a specific source processing during the complicated submarine eruption and suggest that the presence of water plays an important role in interpreting the upward force in the following section.

3 Discussion

3.1 A dynamical model of the explosive MT and upward force

There exist prevailing eruption mechanisms to explain the sudden expansion in volume, which is associated with the explosive component of this event represented by the explosive MT solution (Figure 4a). The first one is the magma-water interaction (O'Callaghan, 2022), which is known as the fuel-coolant model (Morrissey, 2000). It interprets the large explosion as triggered by a sequence of small explosions resulting from direct contact between hot, uplifting magma and cold seawater. Another plausible volcano explosion model is the gas-compressed explosion (Henley & McNabb, 1978; Henley & Hughes, 2016). More investigations on the explosion mechanism are still required, such as sampling fall-out material and detailed petrological and textural analyses (Vergoz et al., 2022).

However, the physical process associated with the unusual upward force in the composite source is not trivial to explain. The first candidate mechanism for the upward force is the drag force of ascending viscous magma acting on the shallow portion of the conduit (Ohminato et al., 1998; Ukawa & Ohtake, 1987). When the Hunga explosion happened, all materials in the cavern

(Figure 4b) were ejected, but the volcano rim survived. Therefore, these jetting materials (a mixture of lava, water, ash etc.) may apply a drag force to the remaining rim. This drag force is approximately given as $F = 8\pi\eta v l$, where η is the viscosity of the material, v is the velocity of the ascending material, and l is the length of the cylindrical conduit (Ohminato et al., 2006). Here, the viscosity is hard to estimate. If we assume $\eta = 10^5$ Pa s from the lower bound of the andesitic magma, $l = 400$ m, which is about half of the depth of the cavern formed by this eruption (Mackay et al., 2022), and a normal discharge rate $v = 300$ m/s, the upward force is about $\sim 10^{11}$ N. This is two orders of magnitudes smaller than the value obtained in this study.

Another mechanism for generating an upward force is the magma hammer, which was proposed by Zheng et al. (2023) to explain the first stage of all four subevents. In this model, at the beginning stage of eruption, the uprising magma strikes a barrier in the conduit or conduit constriction impede the magma flow so that an upward hammer force is applied to the solid earth. However, the upward force in this study should be related to a process following the explosion, making magma hammer not a suitable candidate.

To coincide with the large magnitude of the upward force from the joint MT and SF inversion, we invoke a rebound force. When a shallow underwater explosion happens (Figure 4a), mostly likely relating the sudden volume change due to gas (either magma-water interaction, or compressed gas explosion), a finite volume of water is uplifted. The volume of uplifted water is estimated assuming a displaced cylinder as

$$V = \frac{\pi d^2 h}{4} \tag{3}$$

where d and h are its diameter and height, respectively. Before eruption, this water cylinder applied a pressure on the seafloor as

$$F = \rho V g, \tag{4}$$

where ρ is the seawater density (~1,027 kg/m^3) and g is the gravitational acceleration (~9.8 m/s^2). We used d=6000 m and h=150 m based on the seafloor measurement before eruption (Mackay et al., 2022). Taking all parameters of the Hunga explosion into account, the force is on the order of magnitude 10^{13} N. Once the water was vertically displaced, the pressure on the seafloor suddenly dropped. Consequently, the solid Earth responded by an upward force of $\sim 10^{13}$ N, a rebound force in Figure 4(c), which agrees well with the force magnitude obtained in this study. This can explain why we observed a significant component of upward force accompanying the submarine volcanic explosion. This mechanism is somewhat different from near-surface or buried nuclear explosions where no single force coexists with the explosions.

However, we cannot exclude the drag force and magma hammer force even though their magnitudes are much smaller than the rebound force. A combination mechanism of these three forces may exist during significant eruptions. The rebound force plays a dominant role in the submarine eruptive process that involves the water column displacement.

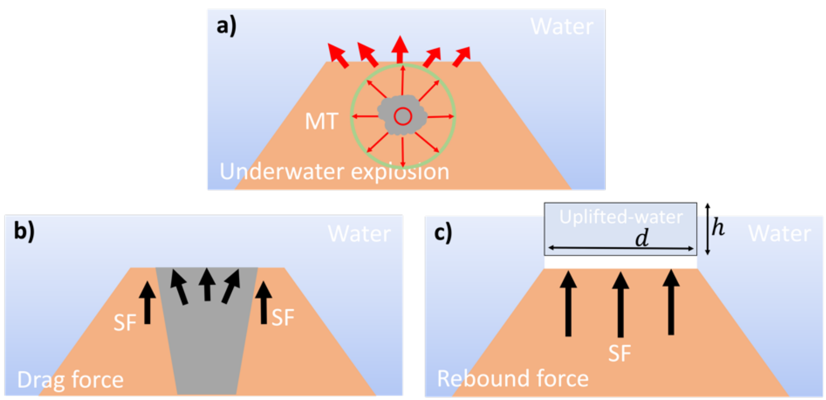

Figure 4: Sketch of models to explain the composite source of explosive MT and upward force. (a) The underwater explosion represented by the explosive MT. (b) The drag force that the jetting materials applied on the wall of the cavern (e.g., Ohminato et al., 2006). (c) The rebound force caused by the abrupt pressure change on the seafloor. The water column is uplifted by an underwater explosion. The pressure on seafloor drops, and the solid Earth responds by an upward rebound force. This happens shortly after the explosion.

3.2 Discussion on structural error

The recovered station-specific time-shifts indicate the 2-D structural effect surrounding the Hunga volcano. To reduce the influence of the inaccurate origin time, we removed the mean of time-shifts. The distribution of calibrated time-shifts is shown in Figure S15. Three stations in the north and east of the volcano require negative time-shifts for the Rayleigh waves, while five stations in the west and south require positive time-shifts. This time-shift distribution agrees with the regional structures (Figure 1a). The structures in the west and south of Hunga volcano are more complicated with a thicker crust, thus positive time-shifts are required because the used ak135f model is too fast. However, the crust in the north and east parts is thinner, the used ak135f model is too slow, requiring negative time-shifts.

4 Conclusion

The seismic data from the first main event of 2022 HTHT eruption can be explained by a composite source of an explosive MT of $M_w = 6.25$ with 62.4% ISO and a striking upward force of 2.0×10^{13} N with a dip angle of -78°. The high percentage of ISO in MT part reveals the explosive nature of this submarine eruption. The SF component is significant because of its high contribution (27%) to the waveforms. To explain the origin of the upward force, we proposed a physical process of the solid earth rebound due to a vertical displacement of the water column above the volcano. The estimated magnitude is about 10^{13} N, which is consistent with the single force amplitude obtained from the joint MT and SF inversion. We realize the explanation of the upward force is challenging and the model of the Hunga eruption remains debatable. This study aims to provide a possible insight on it by engaging a composite source of MT and SF in the seismic source inversion.

Data Availability Statement

Seismic waveforms used in this study are freely downloaded from Incorporated Research Institution for Seismology Data Management Center (IRIS DMC, http://ds.iris.edu/ds/nodes/dmc/) using ObsPy software package (Beyreuther et al., 2010). We use stations from the Global Seismograph Network (IU, https://www.fdsn.org/networks/detail/IU; II, https: //doi.org/10.7914/SN/II) and the Geoscope network(G, https://www.fdsn.org/networks/detail/G). The Green's functions are from the IRIS Data Services product Syngine (Krischer et al., 2017) which manages the database with Instaseis (van Driel et al., 2015).

Acknowledgments

This work was partly supported by DoD AFRL Grant contract number: FA9453-20-C-0072. We use the Python package for Goodman & Weare (2010)'s affine-invariant ensemble sampler, emcee (Foreman-Mackey et al., 2013) to conduct all inversions here. The scattering posterior plots are plotted with corner package (Foreman-Mackey, 2016). All the figures are made with Matplotlib (Hunter, 2007). This work has benefited from some insightful discussions with Dr. Richard Henley.

References

Beyreuther, M., Barsch, R., Krischer, L., Megies, T., Behr, Y., & Wassermann, J. (2010). ObsPy: A Python Toolbox for Seismology. *Seismological Research Letters*, *81*(3), 530–533. https://doi.org/10.1785/gssrl.81.3.530

Carvajal, M., Sepúlveda, I., Gubler, A., & Garreaud, R. (2022). Worldwide Signature of the 2022 Tonga Volcanic Tsunami. *Geophysical Research Letters*, *49*(6), e2022GL098153. https://doi.org/10.1029/2022GL098153

Chouet, B., Dawson, P., Ohminato, T., Martini, M., Saccorotti, G., Giudicepietro, F., et al. (2003). Source mechanisms of explosions at Stromboli Volcano, Italy, determined from moment-tensor inversions of very-long-period data. *Journal of Geophysical Research: Solid Earth*, *108*(B1), ESE 7-1-ESE 7-25. https://doi.org/10.1029/2002JB001919

Dettmer, J., Dosso, S. E., & Holland, C. W. (2007). Uncertainty estimation in seismo-acoustic reflection travel time inversion. *The Journal of the Acoustical Society of America*, *122*(1), 161–176. https://doi.org/10.1121/1.2736514

Donner, S., Steinberg, A., Lehr, J., Pilger, C., Hupe, P., Gaebler, P., et al. (2023). The January 2022 Hunga Volcano explosive eruption from the multitechnological perspective of CTBT monitoring. *Geophysical Journal International*, *235*(1), 48–73. https://doi.org/10.1093/gji/ggad204

Dreger, D. S., Tkalčić, H., & Johnston, M. (2000). Dilational Processes Accompanying Earthquakes in the Long Valley Caldera. *Science*, *288*(5463), 122–125. https://doi.org/10.1126/science.288.5463.122

van Driel, M., Krischer, L., Stähler, S. C., Hosseini, K., & Nissen-Meyer, T. (2015). Instaseis: instant global seismograms based on a broadband waveform database. *Solid Earth*, *6*(2), 701–717. https://doi.org/10.5194/se-6-701-2015

Duputel, Z., & Rivera, L. (2019). The 2007 caldera collapse of Piton de la Fournaise volcano: Source process from very-long-period seismic signals. *Earth and Planetary Science Letters*, *527*, 115786. https://doi.org/10.1016/j.epsl.2019.115786

Foreman-Mackey, D. (2016). corner.py: Scatterplot matrices in Python. *Journal of Open Source Software*, *1*(2), 24. https://doi.org/10.21105/joss.00024

Foreman-Mackey, D., Hogg, D. W., Lang, D., & Goodman, J. (2013). emcee: The MCMC Hammer. *Publications of the Astronomical Society of the Pacific*, *125*(925), 306–312. https://doi.org/10.1086/670067

Garza-Girón, R., Lay, T., Pollitz, F., Kanamori, H., & Rivera, L. (2023). Solid Earth–atmosphere interaction forces during the 15 January 2022 Tonga eruption. *Science Advances*, *9*(2), eadd4931. https://doi.org/10.1126/sciadv.add4931

Goodman, J., & Weare, J. (2010). Ensemble samplers with affine invariance. *Communications in Applied Mathematics and Computational Science*, *5*(1), 65–80. https://doi.org/10.2140/camcos.2010.5.65

Hejrani, B., & Tkalčić, H. (2020). Resolvability of the Centroid-Moment-Tensors for Shallow Seismic Sources and Improvements From Modeling High-Frequency Waveforms. *Journal of Geophysical Research: Solid Earth*, *125*(7). https://doi.org/10.1029/2020JB019643

Henley, R. W., & McNabb, A. (1978). Magmatic vapor plumes and ground-water interaction in porphyry copper emplacement. *Economic Geology*, *73*(1), 1–20. https://doi.org/10.2113/gsecongeo.73.1.1

Henley, Richard W., & Hughes, G. O. (2016). SO 2 flux and the thermal power of volcanic eruptions. *Journal of Volcanology and Geothermal Research*, *324*, 190–199. https://doi.org/10.1016/j.jvolgeores.2016.04.024

Hu, J., Phạm, T.-S., & Tkalčić, H. (2023). Seismic moment tensor inversion with theory errors from 2-D Earth structure: implications for the 2009–2017 DPRK nuclear blasts. *Geophysical Journal International*, *235*(3), 2035–2054. https://doi.org/10.1093/gji/ggad348

Hunter, J. D. (2007). Matplotlib: A 2D Graphics Environment. *Computing in Science & Engineering*, *9*(3), 90–95. https://doi.org/10.1109/MCSE.2007.55

Julian, B. R., Miller, A. D., & Foulger, G. R. (1998). Non-double-couple earthquakes 1. Theory. *Reviews of Geophysics*, *36*(4), 525–549. https://doi.org/10.1029/98RG00716

Kanamori, H., & Given, J. W. (1982). Analysis of long-period seismic waves excited by the May 18, 1980, eruption of Mount St. Helens—A terrestrial monopole? *Journal of Geophysical Research: Solid Earth*, *87*(B7), 5422–5432. https://doi.org/10.1029/JB087iB07p05422

Kanamori, H., Given, J. W., & Lay, T. (1984). Analysis of seismic body waves excited by the Mount St. Helens eruption of May 18, 1980. *Journal of Geophysical Research: Solid Earth*, *89*(B3), 1856–1866. https://doi.org/10.1029/JB089iB03p01856

Kawakatsu, H. (1996). Observability of the isotropic component of a moment tensor. *Geophysical Journal International*, *126*(2), 525–544. https://doi.org/10.1111/j.1365-246X.1996.tb05308.x

Krischer, L., Hutko, A. R., van Driel, M., Stähler, S., Bahavar, M., Trabant, C., & Nissen-Meyer, T. (2017). On-Demand Custom Broadband Synthetic Seismograms. *Seismological Research Letters*, *88*(4), 1127–1140. https://doi.org/10.1785/0220160210

Kubota, T., Saito, T., & Nishida, K. (2022). Global fast-traveling tsunamis driven by atmospheric Lamb waves on the 2022 Tonga eruption. *Science*, *377*(6601), 91–94. https://doi.org/10.1126/science.abo4364

Lanza, F., & Waite, G. P. (2018). Nonlinear Moment-Tensor Inversion of Repetitive Long-Periods Events Recorded at Pacaya Volcano, Guatemala. *Frontiers in Earth Science*, *6*. https://doi.org/10.3389/feart.2018.00139

Lynett, P., McCann, M., Zhou, Z., Renteria, W., Borrero, J., Greer, D., et al. (2022). Diverse tsunamigenesis triggered by the Hunga Tonga-Hunga Ha’apai eruption. *Nature*, *609*(7928), 728–733. https://doi.org/10.1038/s41586-022-05170-6

Mackay, K., Clark, M. R., Seabrook, S., Armstrong, E., Barr, N. G., Frontin-Rollet, G., et al. (2022). *Environmental impacts of the 2022 eruption of Hunga Tonga - Hunga Ha'apai: voyage report of part 1 of the TesMAP survey of the region in April-May 2022 (TAN2206)*. Wellington: National Institute of Water & Atmospheric Research Ltd.

Matoza, R. S., Fee, D., Assink, J. D., Iezzi, A. M., Green, D. N., Kim, K., et al. (2022). Atmospheric waves and global seismoacoustic observations of the January 2022 Hunga eruption, Tonga. *Science*, *377*(6601), 95–100. https://doi.org/10.1126/science.abo7063

Montagner, J.-P., & Kennett, B. L. N. (1996). How to reconcile body-wave and normal-mode reference earth models. *Geophysical Journal International*, *125*(1), 229–248. https://doi.org/10.1111/j.1365-246X.1996.tb06548.x

Morrissey, M. (2000). Phreatomagmatic fragmentation. *Encyclopedia of Volcanoes*, 431–445.

Mustać, M., & Tkalčić, H. (2016). Point source moment tensor inversion through a Bayesian hierarchical model. *Geophysical Journal International*, *204*(1), 311–323. https://doi.org/10.1093/gji/ggv458

Mustać, M., & Tkalčić, H. (2017). On the Use of Data Noise as a Site-Specific Weight Parameter in a Hierarchical Bayesian Moment Tensor Inversion: The Case Study of The Geysers and Long Valley Caldera Earthquakes. *Bulletin of the Seismological Society of America*, ssabull;0120160379v1. https://doi.org/10.1785/0120160379

Mustać, M., Tkalčić, H., & Burky, A. L. (2018). The Variability and Interpretation of Earthquake Source Mechanisms in The Geysers Geothermal Field From a Bayesian Standpoint Based on the Choice of a Noise Model. *Journal of Geophysical Research: Solid Earth*, *123*(1), 513–532. https://doi.org/10.1002/2017JB014897

Mustać, M., Hejrani, B., Tkalčić, H., Kim, S., Lee, S.-J., & Cho, C.-S. (2020). Large Isotropic Component in the Source Mechanism of the 2013 Democratic People's Republic of Korea Nuclear Test Revealed via a Hierarchical Bayesian Inversion. *Bulletin of the Seismological Society of America*, *110*(1), 166–177. https://doi.org/10.1785/0120190062

Ohminato, T., Chouet, B. A., Dawson, P., & Kedar, S. (1998). Waveform inversion of very long period impulsive signals associated with magmatic injection beneath Kilauea volcano, Hawaii. *Journal of Geophysical Research: Solid Earth*, *103*(B10), 23839–23862. https://doi.org/10.1029/98JB01122

Ohminato, T., Takeo, M., Kumagai, H., Yamashina, T., Oikawa, J., Koyama, E., et al. (2006). Vulcanian eruptions with dominant single force components observed during the Asama 2004 volcanic activity in Japan. *Earth, Planets and Space*, *58*(5), 583–593. https://doi.org/10.1186/BF03351955

Omira, R., Ramalho, R. S., Kim, J., González, P. J., Kadri, U., Miranda, J. M., et al. (2022). Global Tonga tsunami explained by a fast-moving atmospheric source. *Nature*, *609*(7928), 734–740. https://doi.org/10.1038/s41586-022-04926-4

Phạm, T.-S., & Tkalčić, H. (2021). Toward Improving Point-Source Moment-Tensor Inference by Incorporating 1D Earth Model's Uncertainty: Implications for the Long Valley Caldera Earthquakes. *Journal of Geophysical Research: Solid Earth*, *126*(11), e2021JB022477. https://doi.org/10.1029/2021JB022477

Poli, P., & Shapiro, N. M. (2022). Rapid Characterization of Large Volcanic Eruptions: Measuring the Impulse of the Hunga Tonga Ha'apai Explosion From Teleseismic Waves. *Geophysical Research Letters*, *49*(8), e2022GL098123. https://doi.org/10.1029/2022GL098123

Proud, S. R., Prata, A. T., & Schmauß, S. (2022). The January 2022 eruption of Hunga Tonga-Hunga Ha'apai volcano reached the mesosphere. *Science*, *378*(6619), 554–557. https://doi.org/10.1126/science.abo4076

Purkis, S. J., Ward, S. N., Fitzpatrick, N. M., Garvin, J. B., Slayback, D., Cronin, S. J., et al. (2023). The 2022 Hunga-Tonga megatsunami: Near-field simulation of a once-in-a-century event. *Science Advances*, *9*(15), eadf5493. https://doi.org/10.1126/sciadv.adf5493

Sambridge, M., Gallagher, K., Jackson, A., & Rickwood, P. (2006). Trans-dimensional inverse problems, model comparison and the evidence. *Geophysical Journal International*, *167*(2), 528–542. https://doi.org/10.1111/j.1365-246X.2006.03155.x

Schimmel, M., & Paulssen, H. (1997). Noise reduction and detection of weak, coherent signals through phase-weighted stacks. *Geophysical Journal International*, *130*(2), 497–505. https://doi.org/10.1111/j.1365-246X.1997.tb05664.x

Tape, W., & Tape, C. (2012). A geometric setting for moment tensors: A geometric setting for moment tensors. *Geophysical Journal International*, *190*(1), 476–498. https://doi.org/10.1111/j.1365-246X.2012.05491.x

Tarumi, K., & Yoshizawa, K. (2023). Eruption sequence of the 2022 Hunga Tonga-Hunga Ha'apai explosion from back-projection of teleseismic P waves. *Earth and Planetary Science Letters*, *602*, 117966. https://doi.org/10.1016/j.epsl.2022.117966

Thurin, J, & Tape, C. (2023). Comparison of force and moment tensor estimations of subevents during the 2022 Hunga–Tonga submarine volcanic eruption. *Geophysical Journal International*, *235*(2), 1959–1981. https://doi.org/10.1093/gji/ggad323

Thurin, Julien, Tape, C., & Modrak, R. (2022). Multi-Event Explosive Seismic Source for the 2022 Mw 6.3 Hunga Tonga Submarine Volcanic Eruption. *The Seismic Record*, *2*(4), 217–226. https://doi.org/10.1785/0320220027

Tkalčić, H., Dreger, D. S., Foulger, G. R., & Julian, B. R. (2009). The Puzzle of the 1996 Bardarbunga, Iceland, Earthquake: No Volumetric Component in the Source Mechanism. *Bulletin of the Seismological Society of America*, *99*(5), 3077–3085. https://doi.org/10.1785/0120080361

Uhira, K., & Takeo, M. (1994). The source of explosive eruptions of Sakurajima volcano, Japan. *Journal of Geophysical Research: Solid Earth*, *99*(B9), 17775–17789. https://doi.org/10.1029/94JB00990

Ukawa, M., & Ohtake, M. (1987). A monochromatic earthquake suggesting deep-seated magmatic activity beneath the Izu-Ooshima Volcano, Japan. *Journal of Geophysical Research: Solid Earth*, *92*(B12), 12649–12663. https://doi.org/10.1029/JB092iB12p12649

USGS. (2022). M 5.8 Volcanic Eruption - 68 km NNW of Nukuʻalofa, Tonga. Retrieved November 3, 2023, from https://earthquake.usgs.gov/earthquakes/eventpage/us7000gc8r/executive

Vasyura-Bathke, H, Dettmer, J., Dutta, R., Mai, P. M., & Jónsson, S. (2021). Accounting for theory errors with empirical Bayesian noise models in nonlinear centroid moment tensor estimation. *Geophysical Journal International*, *225*(2), 1412–1431. https://doi.org/10.1093/gji/ggab034

Vasyura-Bathke, Hannes, Dettmer, J., Steinberg, A., Heimann, S., Isken, M. P., Zielke, O., et al. (2020). The Bayesian Earthquake Analysis Tool. *Seismological Research Letters*, *91*(2A), 1003–1018. https://doi.org/10.1785/0220190075

Vergoz, J., Hupe, P., Listowski, C., Le Pichon, A., Garcés, M. A., Marchetti, E., et al. (2022). IMS observations of infrasound and acoustic-gravity waves produced by the January 2022 volcanic eruption of Hunga, Tonga: A global analysis. *Earth and Planetary Science Letters*, *591*, 117639. https://doi.org/10.1016/j.epsl.2022.117639

Yuen, D. A., Scruggs, M. A., Spera, F. J., Zheng, Y., Hu, H., McNutt, S. R., et al. (2022). Under the surface: Pressure-induced planetary-scale waves, volcanic lightning, and gaseous clouds caused by the submarine eruption of Hunga Tonga-Hunga Ha’apai volcano. *Earthquake Research Advances*, *2*(3), 100134. https://doi.org/10.1016/j.eqrea.2022.100134

Zhao, L.-S., & Helmberger, D. V. (1994). Source Estimation from Broadband Regional Seismograms. *Bulletin of the Seismological Society of America*, *84*(1), 91–104.

Zheng, Y., Hu, H., Spera, F. J., Scruggs, M., Thompson, G., Jin, Y., et al. (2023). Episodic Magma Hammers for the 15 January 2022 Cataclysmic Eruption of Hunga Tonga-Hunga Ha'apai. *Geophysical Research Letters*, *50*(8), e2023GL102763. https://doi.org/10.1029/2023GL102763

Zhu, L., & Helmberger, D. V. (1996). Advancement in source estimation techniques using broadband regional seismograms. *Bulletin of the Seismological Society of America*, *86*(5), 1634–1641. https://doi.org/10.1785/BSSA0860051634